Highly uniform YF$_3$:Ln^{3+} (Ln = Ce^{3+}, Tb^{3+}) walnut-like microcrystals: Hydrothermal synthesis and luminescent properties

Xiaojie Wang [a,b], Tianqi Sheng [a,b], Zuoling Fu [a,b,*], Wenhao Li [c], Jung Hyun Jeong [d,**]

[a] State Key Laboratory of Superhard Materials, College of Physics, Jilin University, Changchun 130012, China
[b] Key Lab of Coherent Light, Atomic and Molecular Spectroscopy, Ministry of Education, Changchun 130012, China
[c] Changchun Institute of Optics, Fine Mechanics and Physics, Chinese Academy of Sciences, Changchun 130033, China
[d] Department of Physics, Pukyong National University, Busan 608-737, South Korea

A B S T R A C T

Uniform and well-crystallized YF$_3$ walnut-like microcrystals were prepared by a facile one-step hydrothermal synthesis. The crystalline phase, size, morphology, and luminescence properties were characterized using powder X-ray diffraction (XRD), field emission-scanning electron microscopy (FE-SEM), transmission electron microscopy (TEM), photoluminescence (PL) and photoluminescent excitation spectra (PLE). The results revealed that the existence of Ce^{3+} (sensitizer) can dramatically enhance green emission centered at 545 nm of Tb^{3+} (activator) in codoped samples due to an efficient energy transfer from Ce^{3+} to Tb^{3+}. The critical energy transfer distance between Ce^{3+} and Tb^{3+} was also calculated by methods of concentration quenching and spectral overlapping. Experimental analysis and theoretical calculations indicated that the dipole–dipole interaction should be the dominant mechanism for the Ce^{3+}–Tb^{3+} energy transfer.

© 2013 Elsevier Ltd. All rights reserved.

1. Introduction

The synthesis of micro- and nanoscale inorganic materials with a special size, morphology including hierarchical structures has gained much attention due to their fundamental scientific interest and potential technological applications in different fields such as photochemistry, superconductors, optoelectronics, solar cells, and catalysis [1–3]. Therefore, tunable or controllable morphology of nano/microcrystals remains an important goal of modern materials chemistry. Many recent efforts have been devoted to the controllable morphology and spatial patterning of various materials, which is a crucial step toward the realization of functional nanosystems [4–7]. Generally, for obtaining different morphologies, chemical vapor deposition [8–12] or solution-phase chemical routes [13–15] have been used, however, they usually require catalysts, expensive and even toxic templates or surfactants, high temperature, and a series of complicated procedures. Therefore, it is still a big challenge to develop simple and reliable synthetic methods for hierarchical architectures with designed chemical components and controlled morphologies, which strongly affect the properties of nano/micromaterials.

YF$_3$ is a very important metal fluoride with potential applications as phosphors [16], ionic conductors [17], and scintillators [18]. YF$_3$ has been used as a host crystal for lanthanide-doped phosphors with interesting down/up conversion luminescent properties [16,19–22]. However, the YF$_3$ crystals obtained are almost irregular nanoparticles. Since the properties of inorganic structures may be well tuned by tailoring the morphology and crystallinity, the crystal structure and crystallization have turned out to affect the optical properties of the luminescent centers [22–24]. Some efforts have been devoted to the synthesis of inorganic microcrystals and nanocrystals with well-defined nonspherical morphologies. Recently, YF$_3$ nanoparticles with quadrilateral and hexagonal shapes have been synthesized using a reverse micro-emulsion technique [25]. Truncated octahedral submicrocrystals and nanocrystals of YF$_3$:Eu^{3+} have been prepared by a Na$_2$H$_2$EDTA-assisted hydrothermal route [26,27]. Spherical and rod europium fluoride nanoparticles were prepared in different tetrafluoroborate ionic liquids [28]. Sodium rare-earth fluoride nanocrystals were also synthesized through co-thermolysis of Na(CF$_3$COO) and RE(CF$_3$COO)$_3$ in oleic acid/oleyamine/1-octadecene [29].

However, in our experiment, we realize the one-step hydrothermal synthesis of YF$_3$:Ce^{3+}, Tb^{3+} walnut-like microcrystals without any organic surfactants and research luminescence properties of Ce^{3+} and Tb^{3+} in YF$_3$. Moreover, the energy transfer efficiency from Ce^{3+} to Tb^{3+}, the energy transfer critical distance

* Corresponding author at: State Key Laboratory of Superhard Materials, College of Physics, Jilin University, Changchun 130012, China. Tel.: +86 431 85167966; fax: +86 431 85167966.
** Corresponding author.
E-mail addresses: zlfu@jlu.edu.cn (Z. Fu), jhjeong@pknu.ac.kr (J.H. Jeong).

(R_c) between Ce^{3+} and Tb^{3+}, and the energy transfer mechanism of Ce^{3+}–Tb^{3+} in YF_3:Ce^{3+}, Tb^{3+} microcrystals have been discussed in detail.

2. Experimental

2.1. Synthesis of the samples

2.1.1. Materials

All reagents were analytically pure, produced by Beijing Chemical Reagent Plant, and used without further purification. The sodium fluoride (NaF) was used as the fluoride source. Rare earth chlorate and rare earth nitrate were used to offer the yttrium, terbium and cerium source, respectively, and they were made into 0.1 mol/ml YCl_3, 0.1 mol/ml $Tb(NO_3)_3$ and 5×10^{-5} mol/ml $Ce(NO_3)_3$ by dissolving appropriate amount of Y_2O_3, CeO_2 and Tb_4O_7 with diluted hydrochloric acid and diluted nitric acid. Meanwhile, aluminum nitrate nonahydrate ($Al(NO_3)_3 \cdot 9H_2O$) were used as the "shape modifiers" [30,31].

2.1.2. Synthesis

In a representative synthesis route, aluminum nitrate non-ahydrate ($Al(NO_3)_3 \cdot 9H_2O$, 3 mmol), 27.9 ml YCl_3, 1.2 ml $Ce(NO_3)_3$ and 1.5 ml $Tb(NO_3)_3$ were mixed together with strong magnetic stirring at room temperature for 20 min. Next the sodium fluoride (NaF, 16.2 mmol) was dissolved in 15 ml distilled water to form aqueous solutions with strong magnetic stirring at room temperature for 20 min to form an aqueous solution. Then the sodium fluoride (NaF) aqueous solution was added dropwise into the above solutions with vigorous stirring at room temperature for 1 h. Finally, the mixture was transferred in a Teflon bottle held in a stainless steel autoclave sealed and maintained at 180 °C for 24 h and cooled naturally to room temperature. The precipitate was washed with deionized water three times. The final products were dried at 65 °C for 12 h in the air.

2.2. Characterization

The structural characteristics of the final products were examined by Powder X-ray diffraction (XRD) pattern using Cu-Kα (λ = 0.15405 nm) radiation on a Rigaku-Dmax 2500 diffractometer. The morphology and the size of the obtained samples were observed with field emission-scanning electron microscopy (FE-SEM, JSM-6700F, JEOL) and transmission electron microscopy (TEM, JEM-2010 JEOL). The ultraviolet–visible photoluminescence excitation and emission spectra were recorded with a Hitachi F-7000 spectrophotometer equipped with Xe-lamp as an excitation. All the measurements were performed at room temperature.

3. Results and discussion

3.1. Crystal structure and morphologies

Fig. 1 presents representative XRD patterns of $Y_{0.98-x}F_3$:$0.02Ce^{3+}$, xTb^{3+} samples with different concentrations after hydrothermal treatment at 180 °C for 24 h. All diffraction peaks can be readily indexed to a pure orthorhombic phase of YF_3 by comparison with the JCPDS card file no. 32-1431. No other impurity peaks are detected in the XRD patterns, it is worth noting that the crystal phase of YF_3 has not been changed after doping with Ce^{3+} and Tb^{3+} ions.

The morphologies and microstructures of the products were investigated by field emission-scanning electron microscopy (FE-SEM), transmission electron microscopy (TEM) and selected-area electron diffraction (SAED). Fig. 2(a) and (b) displays the TEM images of microcrystal, illustrating the morphological evolution of
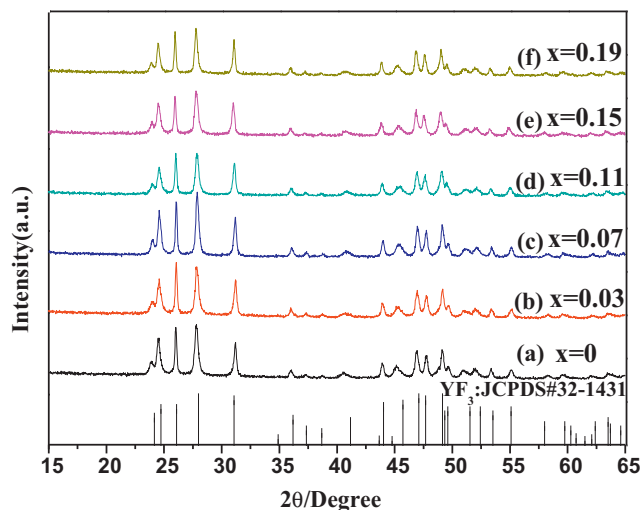

Fig. 1. XRD powder patterns of the $Y_{0.98-x}F_3$:$0.02Ce^{3+}$, xTb^{3+} with different Tb^{3+} concentrations.

the YF_3:Ce^{3+}, Tb^{3+} walnut-like shape. The selected-area electron diffraction (SAED) in Fig. 2(c) exhibited dots, which were due to the diffraction of ensemble microcrystals, indicating that the as-obtained microcrystals were essentially single crystalline in nature. The high-magnified TEM image (Fig. 2(e)) further shows the microcrystals more distinctly. The interplanar distance obtained from the dot is 0.29 nm, which can be assigned to (2 1 0) lattice plane of orthorhombic structure YF_3 (PDF#32-1431). The representative panoramic SEM images shown in Fig. 2(f) and (g) demonstrate that the product is composed of well dispersed particles with small sizes (400–500 nm). The magnified SEM image displayed in Fig. 2(g) indicates that the microcrystals with rough surfaces are piled up by small nanoparticles.

3.2. Luminescence properties

Fig. 3(a) shows the photoluminescence excitation (λ_{em} = 315 nm) and emission (λ_{ex} = 255 nm) spectra of the $Y_{0.98}F_3$:$0.02Ce^{3+}$ microcrystals. Owing to the influences of crystal field splitting and spin–orbit coupling, the 4f → 5d transition of the Ce^{3+} ions will exhibit a subtle structure. The excitation spectrum of the $Y_{0.98}F_3$:$0.02Ce^{3+}$ microcrystals gives a broadband centered at 255 nm with a shoulder centered at 236 nm, which can be attributed to the electric dipole-allowed transitions of the Ce^{3+} ions from the 4f shell to the 5d orbital. With 255 nm radiation, the emission spectrum of $Y_{0.98}F_3$:$0.02Ce^{3+}$ microcrystals exhibits an intense ultraviolet emission band centered at 315 nm, which can be assigned to the 5d–4f electronic transition of the Ce^{3+} ions. Fig. 3(b) shows the excitation (λ_{em} = 545 nm) spectrum of the $Y_{0.89}F_3$:$Ce_{0.02}$, $Tb_{0.09}$ microcrystals and emission (λ_{ex} = 255 nm) spectrum of the $Y_{0.98}F_3$:$0.02Ce^{3+}$ microcrystals. The excitation (λ_{em} = 545 nm) spectrum of $Y_{0.89}F_3$:$Ce_{0.02}$, $Tb_{0.09}$ microcrystals in Fig. 3(b) is similar with the excitation (λ_{em} = 315 nm) spectrum of the $Y_{0.98}F_3$:$Ce_{0.02}$ microcrystals in Fig. 3(a). On the basis of the above excitation spectrum of Tb^{3+} doped samples $Y_{0.89}F_3$:$Ce_{0.02}$, $Tb_{0.09}$ and emission spectra of Tb^{3+} non-doped samples $Y_{0.98}F_3$:$Ce_{0.02}$, we can find that the emission band of Ce^{3+} overlaps well with the excitation band of Tb^{3+}. Therefore, it is expected that a resonance-type energy transfer from Ce^{3+} to Tb^{3+} in Ce^{3+}/Tb^{3+} co-doped YF_3 may occur.

Fig. 4 gives the photoluminescence excitation (λ_{em} = 545 nm) and emission (λ_{ex} = 255 nm) spectra of the $Y_{0.89}F_3$:$Ce_{0.02}$, $Tb_{0.09}$ microcrystals. By monitoring the 545 nm emission of Tb^{3+}, a broad excitation band peaking at 255 nm was shown. With 255 nm
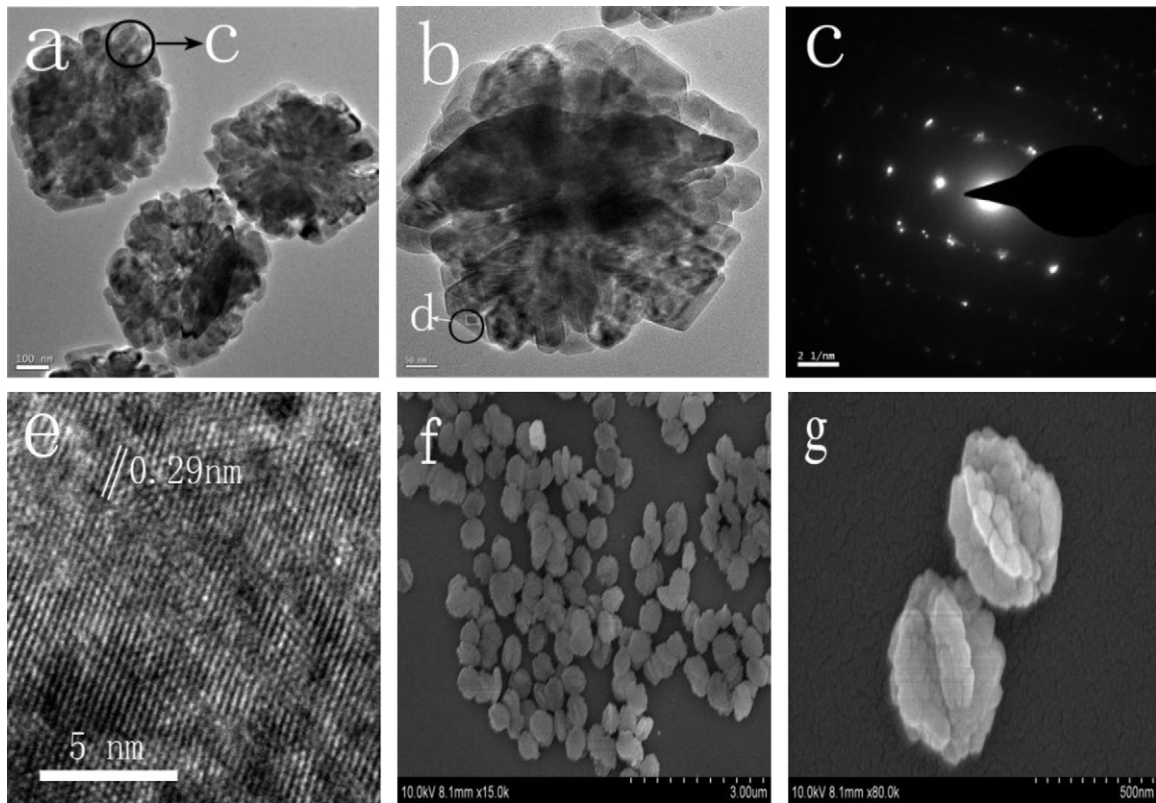
Fig. 2. (a) and (b) TEM images of $YF_3:Ce^{3+}$, Tb^{3+} sample; (c) SAED pattern of the particle; (e) HRTEM image of the sample; (g) and (f) FE-SEM images of the sample.

excitation, the emission spectrum of $Y_{0.89}F_3:Ce_{0.02}$, $Tb_{0.09}$ has characteristic transitions of forbidden 4f–4f transitions within the Tb^{3+} configuration in the wavelength range of 450–650 nm [32–34]. The characteristic emissions of Tb^{3+} at 491, 545, 584 and 621 nm can be attributed to the transitions $^5D_4 \rightarrow {}^7F_6$, $^5D_4 \rightarrow {}^7F_5$, $^5D_4 \rightarrow {}^7F_4$, and $^5D_4 \rightarrow {}^7F_3$, respectively. The green emission ($^5D_4 \rightarrow {}^7F_5$) at 545 nm is more intense than the other transitions because it is a magnetic dipole transition with $\Delta J = 1$ [32].

To explore the possibility of the energy transfer from Ce^{3+} to Tb^{3+} ions, Tb^{3+} ions with different concentrations were doped into the YF_3 microcrystals. Fig. 5 displays the emission spectra of the

$Y_{0.98-x}F_3:0.02Ce^{3+}$, xTb^{3+} microcrystals with different Tb^{3+} concentrations, it contains both the weak emission of the Ce^{3+} ions and the strong green emission of the Tb^{3+} ions. With 255 nm radiation, the emission intensity of the Tb^{3+} ions gradually increases while the emission intensity of Ce^{3+} gradually decreases with the increase of Tb^{3+} doping concentration, indicating that the energy transfer from Ce^{3+} to Tb^{3+} ions is highly efficient since the emission band of the Ce^{3+} ions matches well with the f–f absorptions of the Tb^{3+} ions. Until $Y_{0.85}F_3:Ce_{0.02}$, $Tb_{0.13}$ the emission intensity of Tb^{3+} ions reaches the strongest and then the emission intensity of Tb^{3+} ions gradually decreases with the
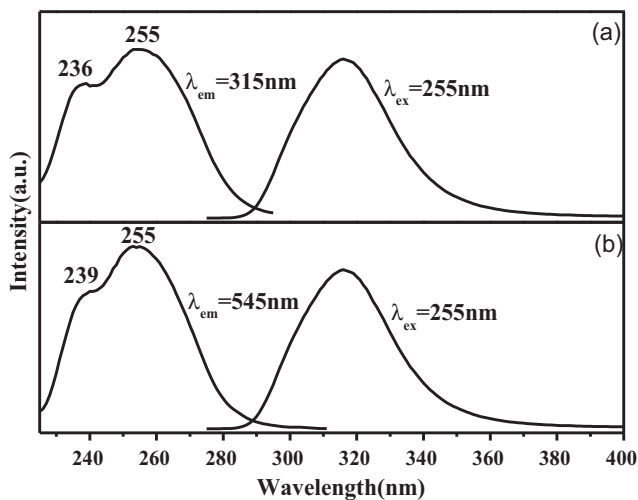

Fig. 3. (a) Excitation (λ_{em} = 315 nm) and emission spectra (λ_{ex} = 255 nm) of the $Y_{0.98}F_3:0.02Ce$ microcrystals. (b) Excitation spectrum (λ_{em} = 545 nm) of the $Y_{0.89}F_3:Ce_{0.02}$, $Tb_{0.09}$ and emission spectrum (λ_{ex} = 255 nm) of the $Y_{0.98}F_3:0.02Ce$ microcrystals.
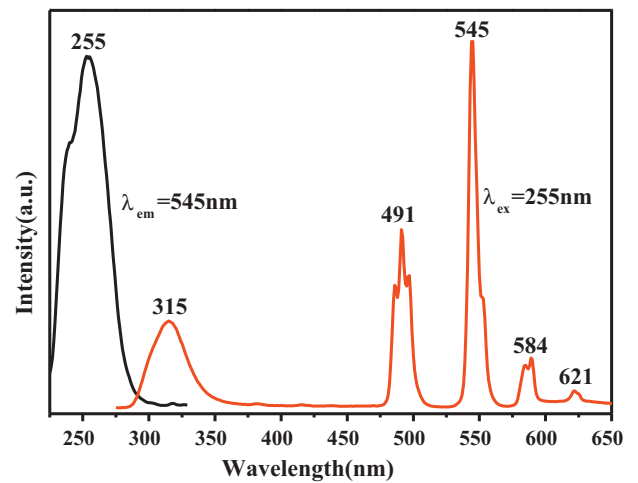

Fig. 4. The photoluminescence excitation (λ_{em} = 545 nm, black line) and emission (λ_{ex} = 255 nm, red line) spectra of the $Y_{0.89}F_3:Ce_{0.02}$, $Tb_{0.09}$ microcrystals. (For interpretation of the references to color in this figure legend, the reader is referred to the web version of this article.)
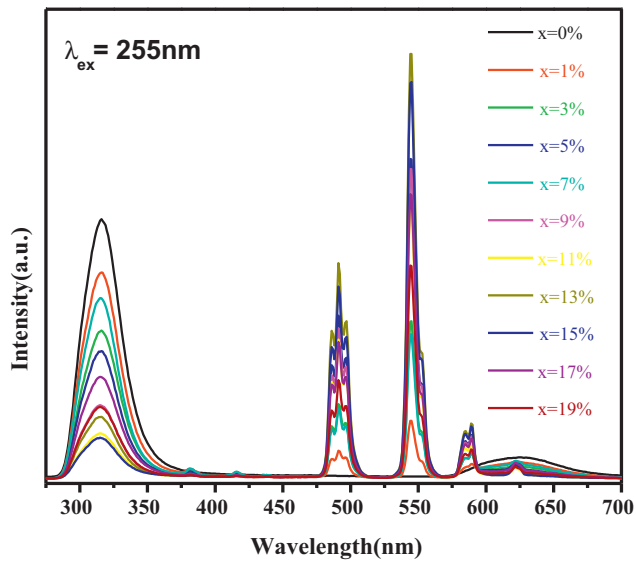
Fig. 5. The emission spectra of the $Y_{0.98-x}F_3$:0.02Ce^{3+}, xTb^{3+} microcrystals with different Tb^{3+} concentrations.

increase of Tb^{3+} doping concentration. The 5d–4f transition of Ce^{3+} is electric-dipole-allowed and is several orders of magnitude stronger than f–f transitions of Tb^{3+}. Therefore, as shown in Fig. 6, the Ce^{3+} ions can strongly absorb UV light from the ground states to the excited states and then transfer energy to Tb^{3+} ions.

On the basis of the above results, Ce^{3+} acts as a sensitizer to yield sensitized luminescence from Tb^{3+} in YF_3. The energy transfer efficiency η_T from Ce^{3+} to Tb^{3+} ions in the $Y_{0.98-x}F_3$:0.02Ce^{3+}, xTb^{3+} microcrystals can be expressed by the following formula [35,36]:

$$\eta_T = 1 - \frac{I_S}{I_{S0}} \tag{1}$$

where I_{S0} and I_S are the intensities of Ce^{3+} in the absence and in the presence of Tb^{3+} respectively. The η_T from Ce^{3+} to Tb^{3+} in $Y_{0.98-x}F_3$:0.02Ce^{3+}, xTb^{3+} microcrystals are calculated and illustrated in Fig. 7 as a function of Tb^{3+} concentration (x). The η_T monotonically increases with increase of Tb^{3+} concentration and is as high as 0.86 when the Tb^{3+} concentration is 0.13. And it has slowly changed after $x = 0.11$ indicating that the η_T has nearly reached the maximum in the sample $Y_{0.85}F_3$:$Ce_{0.02}$, $Tb_{0.13}$.
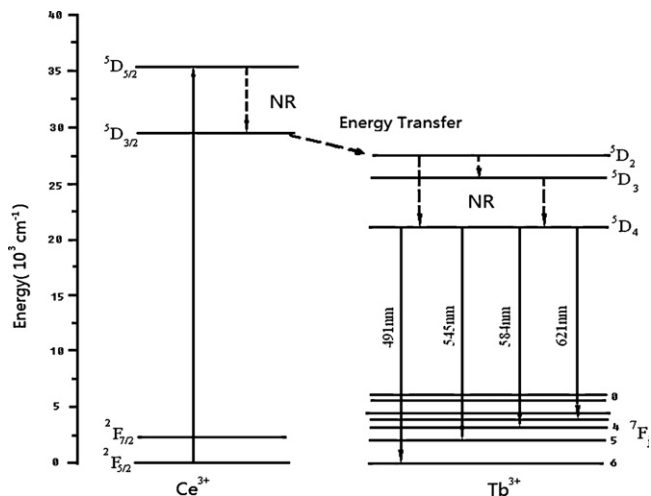

Fig. 6. Energy level scheme for energy transfer process from Ce^{3+} to Tb^{3+} ions in Ce^{3+}–Tb^{3+} codoped YF_3 microcrystals.
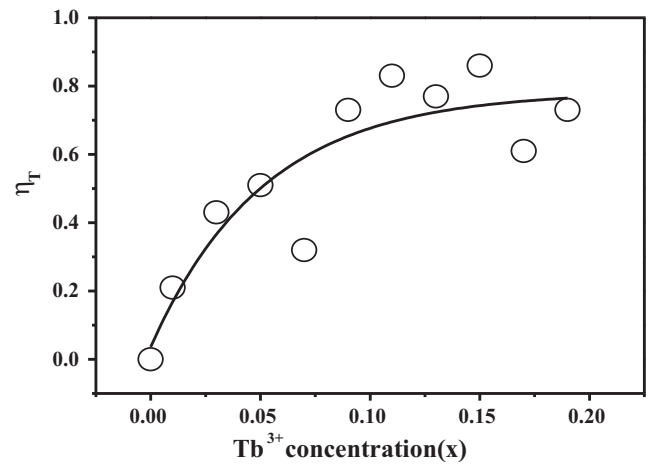

Fig. 7. The energy transfer efficiency η_T from Ce^{3+} to Tb^{3+} ions in the $Y_{0.98-x}F_3$:0.02Ce^{3+}, xTb^{3+} microcrystals.

According to the energy transfer theories of Dexter and Schulman, concentration quenching is due to the energy transfer from one activator to another in many cases until an energy sink in the lattice is reached. As suggested by Blasse [37], the average separation R_{Ce-Tb} can be expressed as follows:

$$R_{Ce-Tb} \approx 2\left(\frac{3V}{4\pi C_{Ce+Tb}N}\right)^{1/3} \tag{2}$$

where N is the number of site that lanthanide ion can occupy in per unit cell, V is the volume of the unit cell, and C_{Ce+Tb} is the total doping concentration of the Ce^{3+} and Tb^{3+} ions. For the host of YF_3, $N = 4$, $V = 191.680$ Å, and Eq. (2) to estimate R_{Ce-Tb}. R_{Ce-Tb} is determined to be 16.6, 14.51, 12.23, 10.94, 10.06, 9.41, 8.90, 8.48, 8.14, 7.84, and 7.58 Å for C_{Ce+Tb} = 0.02, 0.03, 0.05, 0.07, 0.09, 0.11, 0.13, 0.15, 0.17, 0.19, and 0.21, respectively. The critical concentration C_{Ce+Tb} is defined as the concentration for which the emission intensity of the Ce^{3+} ions is half that of the sample in the absence of Tb^{3+} ions. In the host of YF_3 microcrystals, the critical concentration of C_{Ce+Tb} is 0.102 and the corresponding critical distance (R_c) for the Ce^{3+}–Tb^{3+} energy transfer is about 9.65 Å.

The energy transfer from a sensitizer to an activator can take place via radiative energy transfer, exchange interaction, and multipole–multipole interaction. Generally speaking, the existence of radiative energy transfer from a sensitizer to an activator can be confirmed by the spectral dips in the emission spectrum of the sensitizer. The absence of the dips in the emission band of the Ce^{3+} ions corresponding to the f–f absorption lines of the Tb^{3+} ions means that radiative energy transfer between the Ce^{3+} ions and the Tb^{3+} ions can be neglected. Exchange interaction is strongly influenced by the distance between the sensitizer and activator and needs a large overlapping between sensitizer and activator orbitals. While both the Ce^{3+} and Tb^{3+} ions are reducing ions, such an exchange would require very high energy. Generally, the value of the critical distance is about 3–4 Å if the exchange is dominated. In our case, the critical distance of Ce^{3+} and Tb^{3+} is estimated to be 9.65 Å, suggesting that energy transfer via exchange interaction can be excluded either. Thus we suspected that the energy transfer in $Y_{0.98-x}F_3$:0.02Ce^{3+}, xTb^{3+} microcrystals takes place via electric multipole–multipole interaction. On the basis of Dexter's energy transfer formula of multi-polar interaction and Reisfeld's approximation [38–40], the following relation can be given as:
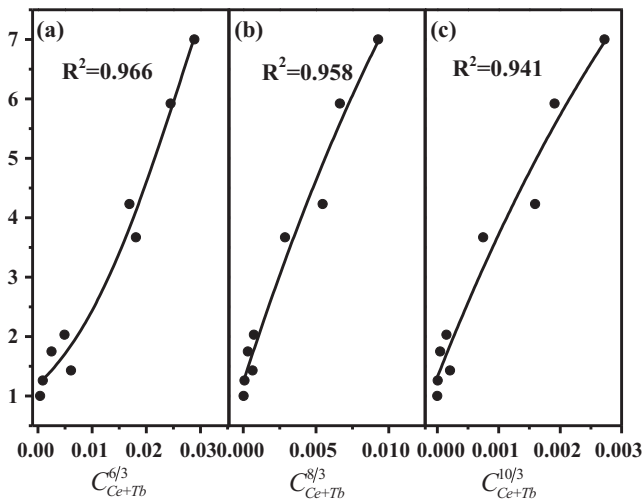
$$\frac{\eta_0}{\eta} \propto C_{Ce+Tb}^{n/3} \tag{3}$$

Fig. 8. Dependence of I_{S0}/I_S of Ce^{3+} on (a) $C_{Ce+Tb}^{6/3}$, (b) $C_{Ce+Tb}^{8/3}$, and (c) $C_{Ce+Tb}^{10/3}$.

Fig. 9. The CIE chromaticity diagram for Y$_{0.98-x}$F$_3$:0.02Ce^{3+}, xTb^{3+} microcrystals with different Tb^{3+} concentrations.

where η_0 and η are the luminescence quantum efficiency of the Ce^{3+} ions in the absence and in the presence of the Tb^{3+} ions, respectively; C_{Ce+Tb} is the total doping concentration of the Ce^{3+} and Tb^{3+} ions; and n = 6, 8, 10 corresponding to dipole–dipole, dipole–quadrupole, and quadrupole–quadrupole interactions, respectively. The value η_0/η can be approximately calculated by the ratio of related luminescence intensities I_{S0}/I_S of Ce^{3+} ions. The $I_{S0}/I_S - C_{Ce+Tb}^{n/3}$ plots are illustrated in Fig. 8 for Y$_{0.98-x}$F$_3$:0.02Ce^{3+}, xTb^{3+}. As n = 6, the curve exhibits the best linear relation in the three plots implying that the energy transfer from Ce^{3+} to Tb^{3+} is considered to be a dipole–dipole mechanism in the YF$_3$ host.

According to Dexter's energy transfer theory, the energy transfer process through multipolar interaction depends on the extent of overlap of the emission spectrum of the sensitizer with the absorption spectrum of the activator, the relative orientation of interacting dipoles and the distance between the sensitizer and the activator. For a dipole–dipole interaction, the energy transfer probability (P_{SA}) from a sensitizer to an activator is given by the following formula:

$$P_{SA}(dd) = \frac{3 \times 10^{12} f_d}{R^6 \tau_s} \int \frac{f_s(E) F_A(E)}{E^4} dE \qquad (4)$$

Here f_d is the oscillator strength of the involved dipole absorption transition of the activator, τ_s is the radiative decay time of the sensitizer, and R is the sensitizer–activator average distance, $f_s(E)$ represents the normalized emission shape function of the sensitizer, and $F_A(E)$ is the normalized absorption shape function of the activator, and E is the energy involved in the transfer (eV).

The critical distance (R_c) of the energy transfer (ET) from the sensitizer to activator is defined as the distance for which the probability of transfer equals the probability of radiative emission of the sensitizer, i.e. the distance for which $P_{SA} \times \tau_s = 1$. Therefore, R_c can be obtained from the formula (4):

$$R_c^6 = 3 \times 10^{12} f_d \int \frac{f_s(E) F_A(E)}{E^4} dE \qquad (5)$$

The f_d of the Tb^{3+} transition is 0.3×10^{-6} [38]. Using this value and the calculated spectral overlap, the critical distance for a dipole–dipole interaction mechanism is estimated to be 10.29 Å, which little deviates from the value estimated from the critical concentration 9.65 Å, indicating that the electric dipole–dipole interaction serves as the main energy transfer mechanism. Besides, the dipole–dipole interaction can generally be expected to
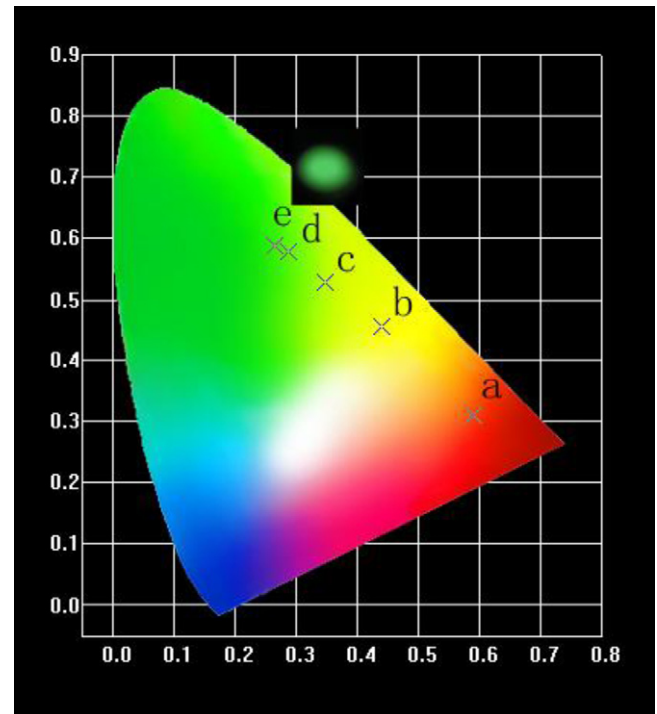
dominate in the energy transfer when both the sensitizer and the activator ions are characterized by electric dipole-allowed transitions, while the f–f transitions of Tb^{3+} are allowed by the selection rules of electric dipole transitions. Further, the dipole–dipole interaction mechanism in the energy transfer can be determined, too. According to the above results, we believe that the energy transfer mechanism from Ce^{3+} to Tb^{3+} in the YF$_3$ host should be predominated by dipole–dipole interaction.

The luminescence color of Y$_{0.98-x}$F$_3$:0.02Ce^{3+}, xTb^{3+} can be tuned by adjusting the doping concentration of Tb^{3+}. Fig. 9 shows the CIE chromaticity diagram for Y$_{0.98-x}$F$_3$:0.02Ce^{3+}, xTb^{3+} microcrystals with different x values. It can be observed that the PL color can be tuned from orange, yellow, to green by changing the doping concentration of Tb^{3+} ions due to different energy transfer efficiencies at different Tb^{3+} concentration. The black dots indicate the CIE chromaticity coordinate positions. The CIE coordinates varied systematically from (0.589, 0.311), (0.439, 0.456), (0.348, 0.527), (0.265, 0.586) to (0.285, 0.586) for x = 0, 0.01, 0.07, 0.13 and 0.19 in Y$_{0.98-x}$F$_3$:0.02Ce^{3+}, xTb^{3+} samples, corresponding to hues ranging from orange to deep green. The inset shows luminescent photograph of the Y$_{0.79}$F$_3$:0.02Ce^{3+}, 0.19Tb^{3+} deep green phosphor under 254 nm excitation. The study opens a novel pathway for tuning the luminescence properties by energy transfer.

4. Conclusion

A simple and facile hydrothermal method was used to prepare YF$_3$ microcrystals. The XRD, FE-SEM and TEM analysis indicated that the samples crystallized in orthorhombic structure with walnut-like morphology and diameter of approximately 400–500 nm. The emission spectra of the Y$_{0.98-x}$F$_3$:0.02Ce^{3+}, xTb^{3+} microcrystals with different Tb^{3+} concentrations demonstrated that energy transfer from the Ce^{3+} to Tb^{3+} ions is highly efficient. The photoluminescence spectra of Y$_{0.98-x}$F$_3$:0.02Ce^{3+}, xTb^{3+} microcrystals shows that the concentration quenching phenomenon occurs when the x = 0.13. The average separation between Ce^{3+}

and Tb^{3+} is calculated and the critical distance R_c is 9.65 Å determined by the method of concentration quenching. The R_c calculated by spectral overlapping method proves this. By comparison of theoretical calculation results to those of experiments, we can infer that the energy transfer from Ce^{3+} to Tb^{3+} in the YF_3 microcrystals occurs predominantly via the dipole–dipole interaction. The as-synthesized luminescent product may have some potential applications in the areas of light display.

Acknowledgements

References

[1] F.E. Osterloh, Chem. Mater. 20 (2008) 35.
[2] C.L. Yan, J. Liu, F. Liu, J.S. Wu, K. Gao, D.F. Xue, Nanoscale Res. Lett. 3 (2008) 473.
[3] R.J. Li, W.P. Hu, Y.Q. Liu, D.B. Zhu, Acc. Chem. Res. 43 (2010) 529.
[4] C.X. Li, J. Yang, P.P. Yang, H.Z. Lian, J. Lin, Chem. Mater. 20 (2008) 4317.
[5] S.H. Yu, J. Yang, Z.H. Han, Y. Zhou, R.Y. Yang, Y.T. Qian, Y.H. Zhang, J. Mater. Chem. 9 (1999) 1283.
[6] X.Q. Chen, S.J. Motojima, Carbon 37 (1999) 1817.
[7] Z.L. Fu, W.W. Xia, Q.S. Li, X.Y. Cui, W.H. Li, CrystEngComm 14 (2012) 4618.
[8] K.K.S. Lau, J.A. Caulfield, K.K. Gleason, Chem. Mater. 12 (2000) 3032.
[9] T. Kawahara, M. Yamamuka, A. Yuuki, K. Ono, Jpn. J. Appl. Phys. 34 (1995) 5077.
[10] J. Kong, A.M. Cassell, H.J. Dai, Chem. Phys. Lett. 292 (1998) 567.
[11] B.S. Kwak, E.P. Boyd, A. Erbil, Appl. Phys. Lett. 53 (1988) 1702.
[12] R.M. Fix, R.G. Gordon, D.M. Hoffman, J. Am. Chem. Soc. 112 (1990) 7833.
[13] B. Cheng, J.M. Russell, W. Sheng, L. Zhang, E.T. Samulski, J. Am. Chem. Soc. 126 (2004) 5972.
[14] S. Fujihara, T. Maeda, H. Ohgi, E. Hosono, H. Lmai, S. Kim, Langmuir 20 (2004) 6476.
[15] J. Joo, J.S. Son, S.G. Kwon, J.H. Yu, T. Hyeon, J. Am. Chem. Soc. 128 (2006) 5632.
[16] Y. Cui, X.P. Fan, Z.L. Hong, M.Q. Wang, J. Nanosci. Nanotechnol. 6 (2006) 830.
[17] S.J. Patwe, P. Balaya, P.S. Goyal, A.K. Tyagi, Mater. Res. Bull. 36 (2001) 1743.
[18] Z.L. Fu, X.Y. Cui, S.B. Cui, X.D. Qi, S.H. Zhou, S.Y. Zhang, J.H. Jeong, CrystEngComm 14 (2012) 3915.
[19] S.L. Zhong, S.J. Wang, H.L. Xu, C.G. Li, Y.X. Huang, S.P. Wang, R. Xu, Mater. Lett. 63 (2009) 530.
[20] M.F. Zhang, H. Fan, B.J. Xi, X.Y. Wang, C. Dong, Y.T. Qian, J. Phys. Chem. C 111 (2007) 6652.
[21] G.F. Wang, W.P. Qin, J.S. Zhang, J.S. Zhang, Y. Wang, C.Y. Cao, J. Phys. Chem. C 112 (2008) 12161.
[22] L.Y. Wang, Y. Zhang, Y.Y. Zhu, Nano Res. 3 (2010) 317.
[23] R.E. Thoma, C.F. Weaver, H.A. Friedman, H. Insley, L.A. Harris, H.A. Yakel Jr., J. Phys. Chem. 65 (1961) 1096.
[24] J.H. Lee, K.H. Ko, B.O. Park, J. Cryst. Growth 247 (2003) 119.
[25] J.L. Lemyre, A.M. Ritcey, Chem. Mater. 17 (2005) 3040.
[26] F. Tao, Z.J. Wang, L.Z. Yao, W.L. Cai, X.G. Li, J. Phys. Chem. C 111 (2007) 3241.
[27] L.W. Qian, J.T. Zai, Z. Chen, J. Zhu, Y.P. Yuan, X.F. Qian, CrystEngComm 12 (2010) 199.
[28] L. Zhu, X.M. Liu, J. Meng, X.Q. Cao, Cryst. Growth Des. 7 (2007) 2505.
[29] H.X. Mai, Y.W. Zhang, L.D. Sun, C.H. Yan, J. Phys. Chem. C 111 (2007) 13730.
[30] X.L. Wu, C.W. Hu, Y.G. Guo, C.W. Hu, J. Phys. Chem. C 112 (2008) 16824.
[31] T. Xia, Q. Li, X.D. Liu, J. Meng, X.Q. Cao, J. Phys. Chem. B 110 (2006) 2006.
[32] T.Q. Sheng, Z.L. Fu, J. Wang, X.H. Fu, Y.N. Yu, S.H. Zhou, S.Y. Zhang, Z.W. Dai, RSC Adv. 2 (2012) 4697.
[33] M.M. Shang, D.L. Geng, Y. Zhang, G.G. Li, D.M. Yang, X.J. Kang, J. Lin, J. Mater. Chem. 22 (2012) 19094.
[34] H.C. Yang, C.Y. Li, Y. Tao, J.H. Xu, G.B. Zhang, Q. Su, J. Lumin. 126 (2007) 196.
[35] G.A. Kumar, P.R. Biju, G. Jose, N.V. Unnikrishnan, Mater. Chem. Phys. 60 (1999) 247.
[36] P.I. Paulose, G. Jose, V. Thomas, N.V. Unnikrishnan, M.K.R. Warrier, J. Phys. Chem. Solids 64 (2003) 841.
[37] G. Blasse, Philips Res. Rep. 24 (1969) 131.
[38] J.M.P.J. Verstegen, J.L. Sommerdijk, J.G. Verriet, J. Lumin. 6 (1973) 425.
[39] G.U. Caldiño, J. Phys.: Condens. Matter 15 (2003) 3821.
[40] D.L. Dexter, J. Chem. Phys. 21 (1953) 836.